Open Ceramics 7 (2021) 100139

Contents lists available at ScienceDirect

Open Ceramics

journal homepage: www.editorialmanager.com/oceram

Direct Ink Writing of cylindrical lattice structures: A proof of concept

Lisa Biasetto [a,*], Giorgia Franchin [b], Hamada Elsayed [b,c], Giovanni Boschetti [a], Kai Huang [b], Paolo Colombo [b,d]

[a] Dipartimento di Tecnica e Gestione Dei Sistemi Industriali, Università di Padova, Stradella San Nicola 3, 36100, Vicenza, Italy
[b] Dipartimento di Ingegneria Industriale, Università di Padova, Via Marzolo 9 35131 Padova, Italy
[c] Refractories, Ceramics and Building Materials Department, National Research Centre, El Buhouth Str., 12622, Cairo, Egypt
[d] Department of Materials Science and Engineering, The Pennsylvania State University, University Park, PA, 16801, USA

ARTICLE INFO

Keywords:
Additive-lathe
4 axis printing
Robotic arm
Polymer-derived ceramics

ABSTRACT

Printing curved lattice structures is a demanding task due to the current limitations in standard 3-axes printing technologies available in the market: a removable support structure often needs to be printed, and printing layer-by-layer to generate an inclined surface causes a significant stair-stepping effect, affecting the surface quality and leading to anisotropy in physical properties. To overcome these limitations, the connection of the printing unit to a >3-axes robotic arm seems to be a feasible solution for printing polymeric based structures, as demonstrated by previous works reported in the literature. In this paper, a method for printing by Direct Ink Writing cylindrical lattice structures is presented: three different materials, SiOC amorphous ceramic, Ti6Al4V-based composite and $CaSiO_3$ bioceramic, are printed by the combination of extrusion of an elastomeric ink and a mandrel connected to a robotic arm. The method shows high potential for printing ceramic and metal cylindrical lattice structures and their combination.

1. Introduction

Among additive manufacturing technologies, Direct Ink Writing (DIW) is one of the most versatile techniques, since it allows printing many classes of materials such as polymers, ceramics, metals and composites. The technique consists in extruding an ink with suitable rheological properties onto a support. The rheology characteristics that an ink must possess for successful DIW printing are: shear thinning (pseudoplastic) behavior with a yield stress, fast recovery times and overall viscosity values compatible with the extrusion equipment and the need to generate structures that do not spontaneously deform under gravity. The pseudoplasticity allows for the ink to flow through the nozzle at low shear stresses, meaning low pressures ($P < 1$ MPa) and/or slow extruder rotation speeds and power (depending on the extrusion equipment used); fast recovery times allow for the printed ink to rapidly transition to a solid-like state before collapsing under its own weight (this is more critical for high density inks, such as metal-based ones) or due to the weight of successive layers.

Usually, a three-axis printer is used, with the printing head in motion whilst the flat support is fixed on the plane. Depending on the ink composition, the printed structure may require different post treatments, such as thermal curing and/or photocuring (elastomers, polymer matrix composites), de-binding and sintering (ceramics and metals). Recently, the use of self-curable polymer binders, such as modified epoxy resin, was explored in order to allow for fast recovery times and higher degree of freedom in shaping [1].

Among polymers, besides the production of biocompatible hydrogels [2], DIW was also used to print highly stretchable elastomers for wearable thermotherapy [3]. Various ceramic compositions have been printed so far, starting form highly loaded polymeric inks where the ceramic phase can be loaded as is or synthesized in-situ during pyrolysis of silicon-based polymers [4], for applications as biomaterials (bone substitutes in non-load bearing applications), filters and catalyst supports. DIW was also tested for printing metallic powders (mainly Ti and Ti based alloys and composites) in the shape of metallic scaffolds [5–8] or more complex structures and various compositions [9,10,11]. Metallic scaffolds of the above compositions were proposed as bone substitutes for load bearing applications.

Very recently, Fused Deposition Modeling printing units have been put on the market (i.e. Markforged Metal X), providing an alternative route for printing metals to the more popular Selective Laser Melting (SLM) or Electron Beam Melting (EBM) technologies.

However, some limitations are associated to the simplicity of the technology and low investment cost of the DIW printing unit, when printing ceramics and metals:

* Corresponding author.
E-mail address: lisa.biasetto@unipd.it (L. Biasetto).

https://doi.org/10.1016/j.oceram.2021.100139
Received 19 March 2021; Received in revised form 28 May 2021; Accepted 31 May 2021
Available online 9 June 2021

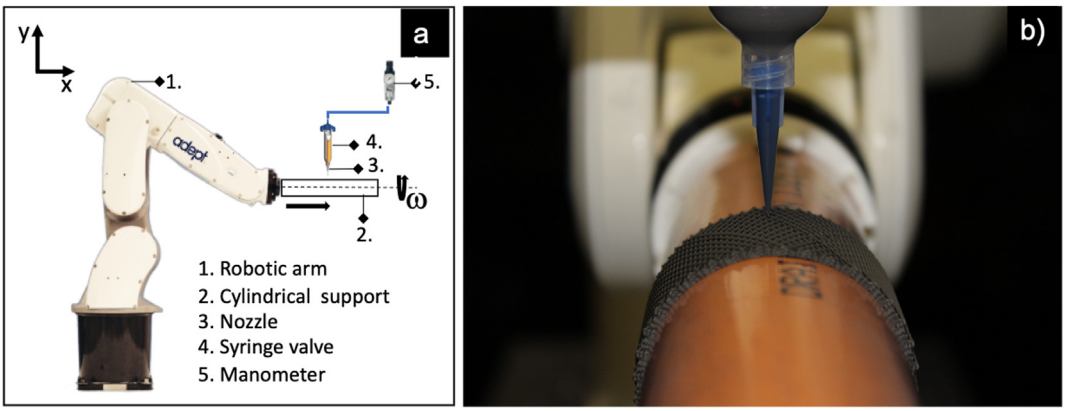

Fig. 1. Schematic representation of the setup used in this work. a) system setup; b) image of a sample during printing.

1) The ink formulation must be strictly controlled in order to achieve the proper rheological properties. For this reason, not all materials can be printed, and a proper ink must be formulated for each material/composition.
2) The binder burn-out may leave behind C, N, O residues that negatively affect the mechanical properties of the metallic structures.
3) The binder burn-out is, for both metals and ceramics, a critical step that can result in cracking and uncomplete densification of the parts.
4) Only three-axis printers have been developed so far for printing metal and ceramic-based DIW inks, thus limiting the range of possible printable geometries.

Furthermore, if metal oxides are used as precursors for metal structures [10], the final component undergoes high volumetric shrinkage (up to 80%).

DIW of elastomers using double curved inflatable surfaces [12,13] or cylindrical mandrels [14] was demonstrated for the production of biomedical devices and dielectric actuators, pneumatic artificial muscles and soft robotics.

In this work, we used elastomeric based inks [15], containing both ceramic and metallic fillers (such as Ti6Al4V powders and $CaSiO_3$ precursors), and we extruded the produced inks onto a rotating and translating cylindrical support (mandrel), using a 5-axes robot. The mandrel could be easily removed, without any thermal or chemical process.

A two-component silicone elastomer, gas-atomized Ti–6Al–4V powders and calcium carbonate powders as calcium oxide precursor for the generation of a $CaSiO_3$ bioceramic, were used as starting materials in different combinations. Different inks were developed for printing 3D porous lattices based on SiOC, titanium alloy (Ti6Al4V) and wollastonite ($CaSiO_3$).

The proposed route shows how complex shapes (cylindrical reticulated structures) of different compositions (SiOC, Ti6Al4V-based composites and $CaSiO_3$) can be produced by DIW, thus widening the range of printable geometries and applications. The movement of the substrate potentially allows for printing in a continuous process; moreover, various extruders could be simultaneously implemented in the same setup, in order to print multi-material components with curved surfaces.

In addition, the use of elastomeric based inks enables an easy removal of the printed structure from the support, and it allows for additional reshaping of the printed structure before pyrolysis and/or sintering.

2. Materials and methods

2.1. Starting materials and ink formulations

A two-component silicone elastomer (PDMS, DOWSIL™ SE 1700, Dow, USA), gas-atomized Ti–6Al–4V powders with size $\leq$10 μm (d_{50}) and purity ~99.7% (TLS Technik Spezialpulver, Bitterfeld, Germany), and calcium carbonate powders ($CaCO_3$, ~10 μm, Industrie Bitossi, Vinci, Italy), as calcium oxide precursor for the generation of a $CaSiO_3$ bioceramic, were used as starting materials in different combinations.

Different inks were developed for printing 3D porous lattices based on SiOC, titanium alloy (TiV4Al6) and wollastonite ($CaSiO_3$), as follows:

a) The silicone adhesive was used as the preceramic polymer precursor generating a SiOC amorphous ceramic after pyrolysis. The ink was prepared by mixing the silicone base (part A) with its proprietary curing agent (part B) at a 10:1 wt ratio, as suggested by the manufacturer [15].

b) For the material based on the titanium alloy (TiV4Al6), the titanium powder was mixed at a ratio of 80:20 wt% into the DOWSIL™ SE 1700 (two-component silicone; Part A and Part B), which was used as a main binder controlling the viscosity of the ink.

c) Calcium carbonate powder was added as an active filler in the DOWSIL™ SE 1700 silicone, to produce wollastonite ($CaSiO_3$) ceramic lattices after the heat treatment [16].

All inks were mixed in a planetary mixer (ARE 250, Thinky, Japan) for 15 min (2000 rpm/min), in order to obtain homogenous pastes without aggregates ensuring a continuous extrusion during the Direct Ink Writing. The inks were then placed into syringes, followed by degassing in the planetary mixer before printing. Then, DIW of all inks was performed at room temperature through conical plastic nozzles (410 μm, Nordson, USA).

2.2. Experimental setup used for the printing process

In Fig. 1, a schematic overview of the printing setup implemented for this work is reported. An Adept Viper Articulated Robotic arm was used in order to move the mandrel both with a translational motion along the x axis and a rotation around the same axis.

The mandrel was a commercially available PVC tube with 38 mm outer diameter. The PVC tube was connected to the printing arm by means of a 3D printed customized plastic support. During the printing operations, the tube was covered by a silicone coated Teflon foil. The syringe was filled with the ink and the piston, and it was connected to the compressed air supply. The positioning of the syringe over the tube was adjusted manually.

The ink was extruded from the nozzle forming 3D patterns layer by layer with well-defined inter-layer spacing (80% of the nozzle diameter), using a gas pressure of 0.3–0.6 MPa. The cylindrical support was moved in the x direction with a speed of 10 mm/s and rotated with a speed of 9 rpm.

In order to achieve the grid pattern shown in Fig. 1b, a proper robotic task was defined and written in the robotic language (Adept V+) suitable for the manipulator employed.

The grid pattern was designed with the purpose of printing empty cylinders with meshed walls with a total height of 60 mm, an internal diameter of 38 mm and a thickness corresponding to 6 layers; each layer

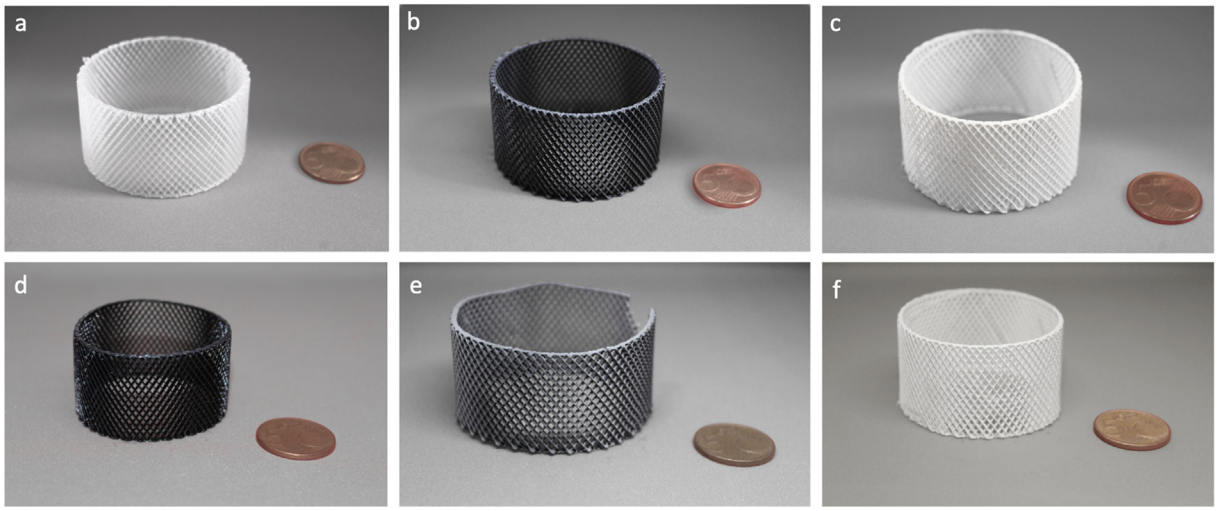

Fig. 2. As printed and cross-linked lattice structures (a) PDMS, b) PDMS plus Ti6Al4V, c) PDMS plus $CaCO_3$); the same structures after pyrolysis (d) SiOC, e) Ti6Al4V composite, f) $CaSiO_3$, sintered in air).

was composed of parallel struts with d ~410 μm crossing the previous one at 45°. Each ink filament of the grid was obtained by imposing a rotation of 45° to the mandrel for each translational movement of 60 mm. Then, a rotation of 5° without translation was used to separate the next filament from the already printed one. At this point, the two movements were repeated until the robot generated a full cylindric structure by performing a 360° rotation. Then, the robot lowered the mandrel with a movement of 0.32 mm (~0.8d) in the negative y axis direction. The next layer was obtained by repeating the same translation movement, imposing a rotation to the mandrel in the opposite direction with respect to the previous one.

It is important to observe that the accuracy of the robot within the work-area used in this experiment (~1 mm) does not allow to achieve the proposed task with the needed precision. For this reason, a proper calibration step was introduced. Moreover, the trajectory planner was set to move the robot with a constant speed and with proper connection arcs

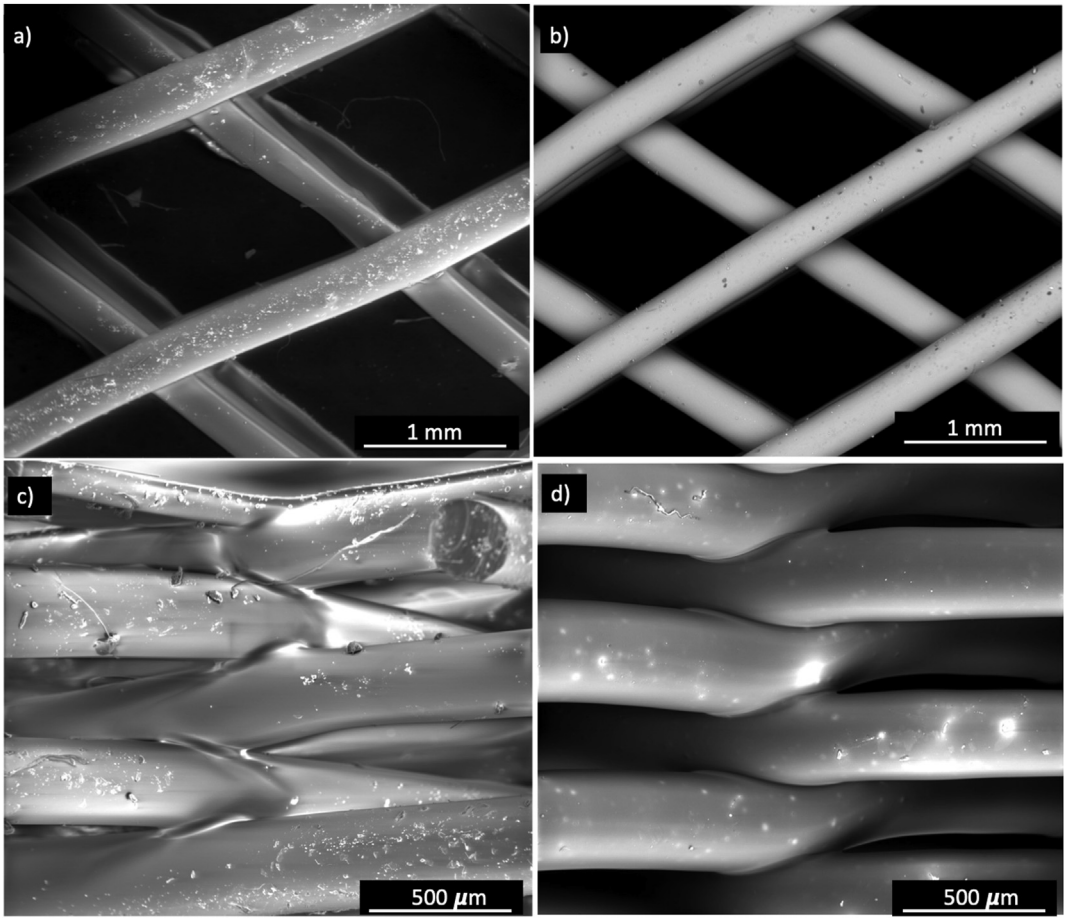

Fig. 3. SEM images of the printed PDMS lattices after crosslinking (a,c) and pyrolysis (b,d).

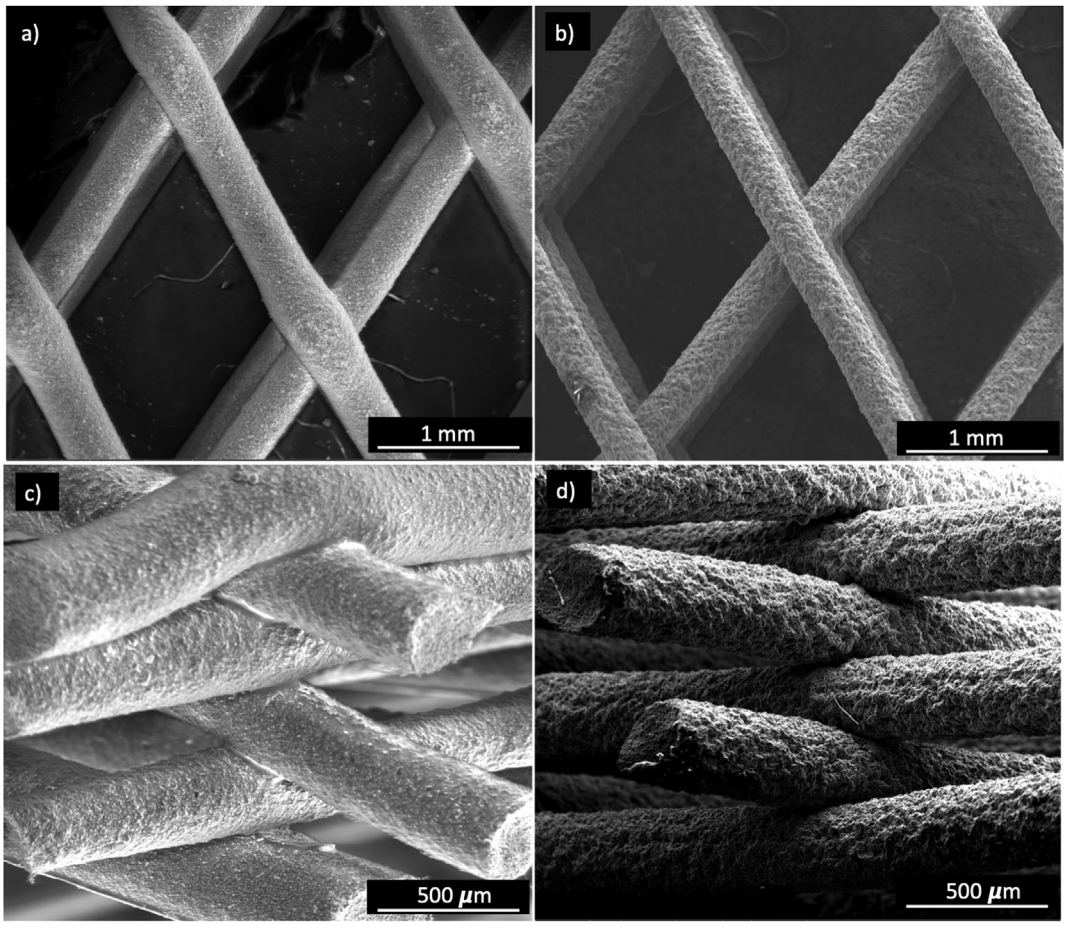

Fig. 4. SEM images of PDMS plus Ti6Al4V lattices after crosslinking (a,c) and of the Ti6Al4V composite lattices after pyrolysis (b,d).

between the paths. This approach enabled the syringe to depose the ink filament on the PVC tube with the required precision.

2.3. Heating and characterization of the printed parts

After the printing process, the lattices were left on the PVC tube and kept at 75 °C for 60 min to solidify through cross-linking of the DOWSIL™ SE 1700 silicone. To produce SiOC lattices, the samples were pyrolyzed at 1000 °C for 2 h with a heating rate of 1 °C/min and an intermediate dwelling step at 300 °C, with a hold time of 3 h. The heat-treatment was carried out in a tube furnace under inert atmosphere (99.99% N_2), and the preceramic cylinders were placed vertically in the ceramic tube without any additional support. The titanium-based lattices were de-binded under high vacuum (10^{-5} mbar), using a heating rate of 0.5 up to 500 °C with 3 h holding time, and then sintered at 1450 °C, for 2 h, under Ar with a heating rate of 2 °C/min. The Ti6Al4V elastomeric lattice was kept on a graphite rod in order to enable shape retention when positioning it horizontally during pyrolysis. This configuration was necessary due to the small size of the tube diameter and crucible, that didn't allow for vertical positioning. The wollastonite lattices were ceramized both in static air and N_2 flow using a heating rate of 0.5 °C up to 1000 °C and a dwelling time of 2 h at the maximum temperature. Again, the preceramic cylinders were placed vertically in the ceramic tube without any support.

The printed parts before and after pyrolysis were visually analysed by field emission gun-scanning electron microscopy (FEG-SEM; Quanta 250 Fei, Eindhoven, The Netherlands) using 20 kV voltage, 5 μm spot size and 10 mm working distance. Ceramic and metallic raw powders, as well as fabricated specimens after the thermal treatments, were analysed by X-ray diffractometry (XRD, Bruker D8 Advance, Milano, Italy) using Cu–Kα radiation at 40 mV and 40 mA, with a resolution of 0.05° for 2 s.

The shrinkage before and after the thermal treatments was measured by Image Analysis software (Image J) on 2D scanned surfaces. At least 5 measurements both for cell size (area) and strut size (diameter) for each composition were performed. The weight loss of the printed parts during the heat treatments was also measured.

3. Results and discussion

In Fig. 2, the three lattices (SiOC, Ti6Al4V-based composite and $CaSiO_3$, respectively) are shown after printing and crosslinking (a-b-c) and after pyrolysis (d-e-f). After printing and crosslinking very well-defined structures were obtained, showing defect-free geometries. During pyrolysis, some distortions occurred, in particular for the SiOC (Fig. 2d) and the Ti6Al4V composite (Fig. 2e) samples. In the case of the SiOC sample, the distortion from the original shape may be derived from the positioning of the sample inside the oven, being the printed lattice highly stretchable even after crosslinking, due to the absence of fillers. In the case of the Ti6Al4V composite sample, the use of the graphite rod during pyrolysis induced stresses in the lattice structure, inhibiting its shrinkage and leading the structure to partial failure. The presence of the reactive $CaCO_3$ fillers in the ink reduced the criticalities upon pyrolysis for the $CaSiO_3$ sample (at least at the macroscopic level), which are mainly due to the volume variation occurring during heating.

Fig. 3 shows SEM images of the PDMS sample after printing and crosslinking (a,c) and pyrolysis (b,d). The as printed structure showed an optimal shape retention that was confirmed at the microscopic level after pyrolysis, when a crack-free structure and smooth surface were obtained. A good adhesion between different filaments can be observed, both before and after pyrolysis.

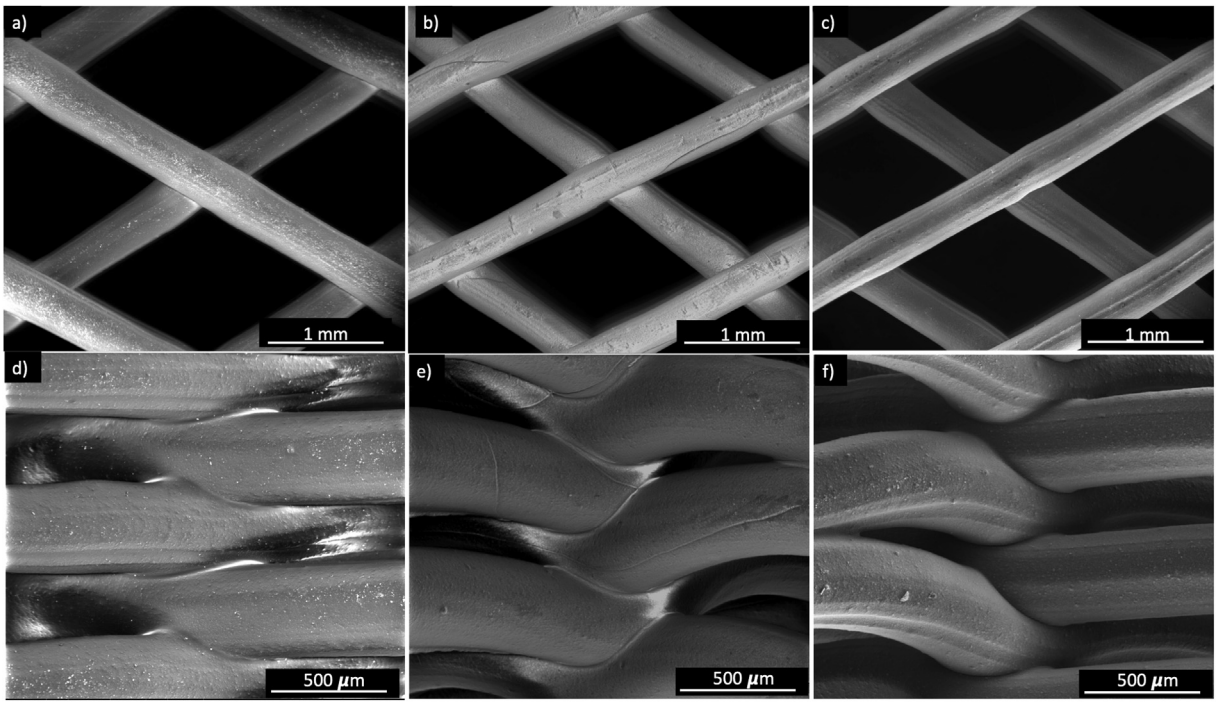

Fig. 5. SEM images of PDMS plus $CaCO_3$ lattices after crosslinking (a,c) and of $CaSiO_3$ lattices after firing in air (b,d) or pyrolysis in N_2 (e,f).

Table 1
Measured linear shrinkage and weight loss of the printed lattice structures after pyrolysis in N_2 or vacuum-Ar, or firing in air.

Sample	Δd% (strut diameter)	ΔA% (cell area)	Δwt %
PDMS (N_2)	30.5 ± 0.1	37.1 ± 1.0	27.5
PDMS + Ti6Al4V (vacuum-Ar)	19.7 ± 2.0	-3.6 ± 0.1	9.5
PDMS + $CaCO_3$ (Air)	15.7 ± 0.4	21.9 ± 0.1	39.0
PDMS + $CaCO_3$ (N_2)	8.7 ± 0.5	22.7 ± 0.1	36.0

In Fig. 4, the PDMS-Ti6Al4V sample after printing and crosslinking is shown (a,c). In this case, the struts show a slight collapse on the adjacent layer (Fig. 4c), probably due to the high density of the metallic powders in the ink. However, after pyrolysis these defects appear to have been compensated by the thermally induced stresses and associated volume shrinkage (Fig. 4b,d). In the final structure, the presence of the Ti6Al4V sintered powders is clearly visible, generating a rough surface. No cracks were visible in the Ti6Al4V composite samples.

In Fig. 5, the PDMS-$CaSiO_3$ lattice is shown after printing and crosslinking (Fig. 5a,d) and after heating in air (Fig. 5b,e) and nitrogen (Fig. 5c,f). After firing, some cracks were visible on the struts' surface of the $CaSiO_3$ lattice heated in air (Fig. 5b,e), whilst a completely crack-free structure was obtained upon pyrolysis under nitrogen flow (Fig. 5c,f). This can be attributed to a reduced shrinkage when pyrolyzing under nitrogen, as reported in Table 1 (8.7% vs 15.7% in air). Firing PDMS in air causes the oxidation of all carbon atoms present in the polymeric chain through an exothermic reaction that can lead to the formation of local cracks, generating highly reactive SiO_2 that can then form $CaSiO_3$ together with the CaO deriving from the thermal decomposition of the $CaCO_3$ powders [16]. When using nitrogen as the pyrolysis atmosphere, carbon atoms are retained in the structure either bonded to Si or as a separate phase, generating a SiOC material with reduced local thermal stresses [16,17.]]. [][][].

This is confirmed by the data reported in Table 1. The struts' diameter shrinkage, as well as the cells' area shrinkage, show different trends: the pure PDMS ink showed a high shrinkage both for struts and cells' area (30.5% and 37.1%, respectively), as expected. The inks containing filler powders showed a limited struts' and cells' area shrinkage (ranging from 8.7% to 15.7% and from -3.6% to 22.7%, respectively). In the case of the PDMS plus $CaCO_3$ ink, a higher strut shrinkage was measured for samples heat treated in air, as discussed above. In the case of the PDMS plus Ti6Al4V ink, the high struts' shrinkage and the negative shrinkage (expansion) can be attributed to the stress induced by the use of the graphite rod upon pyrolysis. The measured weight loss (Table 1) for pure PDMS samples upon pyrolysis is compatible with the organic moieties' elimination and the full conversion of PDMS to a SiOC ceramic. For PDMS plus Ti6Al4V the reduced weight loss during thermal treatment is due to the reaction of Si and C atoms with Ti and V as discussed in the following. The higher weight loss for PDMS plus $CaCO_3$ is compatible with $CaCO_3$ thermal decomposition (with CO_2 emission) that starts occurring at $T > 550$ °C and depends on heating rate and CO_2 concentration in the atmosphere [18].

SEM investigations on the cross-section of the struts of the lattice structures, not reported here for the sake of brevity, showed that air bubbles were not detected in all cases, indicating that the mixing and degassing procedure to produce the inks did not introduce unwanted porosity.

The crystalline phase assemblage of the printed lattice structures after the heat treatment was investigated (Fig. 6). The XRD pattern for the pyrolyzed SiOC is shown in Fig. 6a, where the broad peak is typical of an amorphous material that doesn't contain any crystalline phases. The XRD pattern of the Ti6Al4V-based composite shows, besides the main peaks of titanium metal (PDF#89-3725), the formation of titanium silicide (PDF#78-1429) along with traces of vanadium carbide (PDF#65-3772), see Fig. 6b. The reactivity of Ti6Al4V towards Si and C atoms present in the silicone binder was already observed in our previous work [19]. The presence of calcium silicate crystals is shown in Fig. 6c and d, testifying the reaction between the silicone binder and the calcium carbonate particles in the ink. The only crystal phase that formed after the treatment in air was Wollastonite-2M (PDF#27-0088), along with Pseudo-wollastonite (PDF#89-6463) for the samples heat treated in nitrogen, as already reported in Ref. [4].

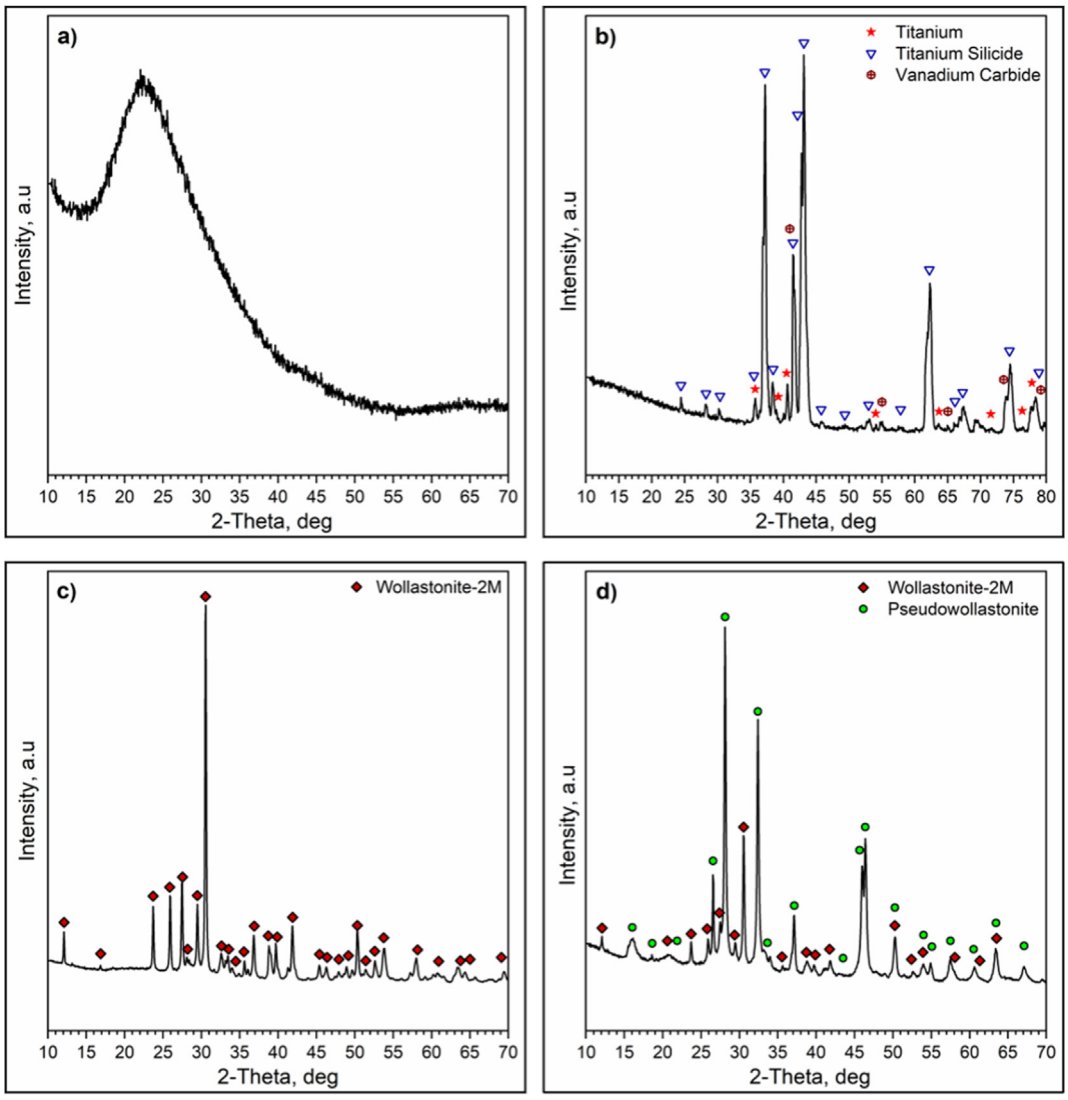

Fig. 6. XRD patterns of the cellular lattices after the heat treatments: a) PDMS after pyrolysis at 1000 °C; b) PDMS plus Ti6Al4V after pyrolysis at 1400 °C; PDMS plus $CaCO_3$ after heating at 1000 °C) in air, d) in nitrogen.

4. Conclusions

In this work, we produced cylindrical lattice structures made of SiOC glass, Ti6Al4V-based composite and $CaSiO_3$ bioceramic, by means of Direct Ink Writing combined with a rotating cylindrical mandrel operated by a robotic arm.

The use of elastomer-based inks allowed printing a highly stretchable structure that could be easily removed from the mandrel without the need of any mechanical or chemical procedures. The printed structures showed sufficient shape retention after curing. Upon heating, the PDMS converted to an amorphous SiOC ceramic, while the PDMS plus Ti6Al4V and PDMS plus $CaCO_3$ inks were converted to a Ti6Al4V-based composite and a $CaSiO_3$ bioceramic, respectively.

For the three compositions tested so far, a satisfactory shape retention after heating was demonstrated, thus showing the high potential of this technology to produce curved lattice components made of glass, ceramic or metal. For metal-based inks, the use of silicon free elastomers is necessary in order to avoid the formation of brittle compounds. The structures here proposed represent a proof of concept of the feasibility of the method and open the way for the production of further curved lattice structures, which are of crucial interest for applications such as highly personalized medicine devices (bone grafts, stents, …) and multi-material components.

Acknowledgments

Authors are grateful to Riccardo Minto, PhD student of Mechatronics, University of Padova for kind assistance during printing operations; Anna De Marzi, PhD student in Industrial Engineering, University of Padova for assistance in image editing and Prof. Gianpaolo Savio, University of Padova for helpful discussion on the experimental setup.

Appendix A. Supplementary data

Supplementary data to this article can be found online at https://doi.org/10.1016/j.oceram.2021.100139.

References

[1] D. Zhang, W. Jonhson, T. Seng Herng, Y. Quan Ang, L. Yang, S. Ching Tan, E. Peng, H. He, J. Ding, A 3D-printing method of fabrication for metals, ceramics, and multi-materials using a universal self-curable technique for robocasting, Mater. Horiz. 7 (2020) 1083–1090, https://doi.org/10.1039/C9MH01690B.

[2] Y. Cheng, K. Hoe Chan, X.-Q. Wang, T. Ding, T. Li, X. Lu, G. Wei Ho, Direct-ink-write 3D printing of hydrogels into biomimetic soft robots, ACS Nano 13 (2019) 13176–13184, https://doi.org/10.1021/acsnano.9b06144.
[3] Y. Wang, Z. Yu, G. Mao, Y. Liu, G. Liu, J. Shang, S. Qu, Q. Chen, R.-W. Li, Printable liquid-metal@PDMS stretchable heater with high stretchability and dynamic stability for wearable thermotherapy, Adv. Mater. Technol. 4 (2019) 1800435, https://doi.org/10.1002/admt.201800435.
[4] A. Zocca, G. Franchin, H. Elsayed, E. Gioffredi, E. Bernardo, P. Colombo, Direct ink writing of a preceramic polymer and fillers to produce hardystonite ($Ca_2ZnSi_2O_7$) bioceramic scaffolds, J. Am. Ceram. Soc. 99 (2016) 1960–1967, https://doi.org/10.1111/jace.14213.
[5] M. Coffigniez, L. Gremmillard, S. Balvay, J. Lachambre, J. Adrien, X. Boulnat, Direct-ink writing of strong and biocompatible titanium scaffolds with bimodal interconnected porosity, Add Man 39 (2021) 101859, https://doi.org/10.1016/j.addma.2021.101859.
[6] B. Song, C. Kenel, D.C. Dunand, 3D ink-extrusion printing and sintering of Ti, Ti-TiB and Ti-TiC microlattices, Add Man 35 (2020) 101412, https://doi.org/10.1016/j.addma.2020.101412.
[7] H. Elsayed, N. Novak, M. Vesenjak, F. Zanini, S. Carmignato, L. Biasetto, The effect of strut size on microstructure and compressive strength of porous Ti6Al4V lattices printed via Direct Ink Writing, Mater. Sci. Eng. 3 (2020) 139484, https://doi.org/10.1016/j.msea.2020.139484.
[8] H. Elsayed, P. Rebesan, G. Giacomello, M. Pasetto, C. Gardin, L. Ferroni, B. Zavan, L. Biasetto, Direct ink writing of porous titanium (Ti6Al4V) lattice structures Mat, Sci & Eng C 103 (2019) 109794, https://doi.org/10.1016/j.msec.2019.109794.
[9] E. Hong, B.Y. Ahn, D. Shoji, J.A. Lewis, D.C. Dunand, Microstructure and mechanical properties of reticulated titanium scrolls, Adv. Eng. Mater. 12 (2011) 1122–1127, https://doi.org/10.1002/adem.201100082.
[10] B.Y. Ahn, D. Shoji, C.J. Hansen, E. Hong, D.C. Dunand, J.A. Lewis, Printed origami strucutres, Adv. Mater. 22 (2010) 2251, https://doi.org/10.1002/adma.200904232.
[11] Shannon L. Taylor, Adam E. Jakus, Ramille N. Shahan, David C. Dunand, Iron and nickel cellular structures by sintering of 3D-printed oxide or metallic particle inks, Adv. Eng. Mater. 19 (2017) 1600365, https://doi.org/10.1002/adem.201600365.
[12] M. Schaffner, J.A. Faber, L. Pianegonda, P.A. Rühs, F. Coulter, A.R. Studart, 3D printing of robotic soft actuators with programmable bioinspired architectures, Nat. Commun. 9 (2018) 145, https://doi.org/10.1038/s41467-018-03216-w.
[13] F. Coulter, B.S. Coulter, E. Papastavrou, A. Ianakiev, Production techniques for 3D printed inflatable elastomer structures: Part II—four-Axis Direct ink writing on irregular double-curved and inflatable surfaces, 3D Print. Addit. Manuf. 5 (2018) 17–28, https://doi.org/10.1089/3dp.2017.0069.
[14] K. Reeser, A.L. Doiron, Three-dimensional printing on a rotating cylindrical mandrel: a review of additive-lathe 3D printing technology 3D printing and add, Manu Tech 6 (2019) 293–307, https://doi.org/10.1089/3dp.2019.0058.
[15] K. Huang, H. Elsayed, G. Franchin, P. Colombo, Complex SiOC ceramics from 2D structures by 3D printing and origami Add, Man (Lond.) 33 (2020) 101144, https://doi.org/10.1016/j.addma.2020.101144.
[16] H. Elsayed, P. Colombo, Crack-free silicate bioceramics from preceramic polymers, Advan in Appl Ceram 115 (2016) 193–199, https://doi.org/10.1080/17436753.2015.1116663.
[17] P. Colombo, G. Mera, R. Riedel, G. Sorarù, Polymer-derived ceramics: 40 Years of research and innovation in advanced ceramics, J. Am. Ceram. Soc. 93 (2010) 1805–1837, https://doi.org/10.1111/j.1551-2916.2010.03876.x.
[18] K.M. Caldwell, P.K. Gallagher, D.W. Johnson Jr., Effect of thermal transport mechanisms on the thermal decomposition of CaCO3, Thermochim. Acta 18 (1977) 15–19, https://doi.org/10.1016/0040-6031(77)80031-2.
[19] A. Fabrizi, F. Bonollo, P. Colombo, L. Biasetto, In situ reinforcement of Ti6Al4V matrix composites by polymer-derived-ceramics phases, Adv. Eng. Mater. 17 (2015) 866–875, https://doi.org/10.1002/adem.201400362.